Crossing a topological phase transition with a quantum computer

Adam Smith,[1, 2, *] Bernhard Jobst,[1] Andrew G. Green,[3] and Frank Pollmann[1, 4]

[1]*Department of Physics, T42, Technische Universität München, James-Franck-Straße 1, D-85748 Garching, Germany*
[2]*Blackett Laboratory, Imperial College London, London SW7 2AZ, United Kingdom*
[3]*London Centre for Nanotechnology, University College London, Gordon St., London WC1H 0AH, United Kingdom*
[4]*Munich Center for Quantum Science and Technology (MCQST), Schellingstr. 4, D-80799 München, Germany*

(Dated: November 21, 2019)

Quantum computers promise to perform computations beyond the reach of modern computers with profound implications for scientific research. Due to remarkable technological advances, small scale devices are now becoming available for use. One of the most apparent applications for such a device is the study of complex many-body quantum systems, where classical computers are unable to deal with the generic exponential complexity of quantum states. Even zero-temperature equilibrium phases of matter and the transitions between them have yet to be fully classified, with topologically protected phases presenting major difficulties. We construct and measure a continuously parametrized family of states crossing a symmetry protected topological phase transition on the IBM Q quantum computers. The simulation that we perform is easily scalable and is a practical demonstration of the utility of near-term quantum computers for the study of quantum phases of matter and their transitions.

There are now many approaches being taken to realise universal quantum computers [1], with numerous academic research groups, companies and governments across the world devoting resources to each. Amongst the most advanced are devices based on trapped ions [2], localized spins in diamond [3] or silicon [4], and superconducting circuits [5, 6]. While each has its advantages—such as coherence times, efficient readout, or gate speeds and fidelities—the latter is fast becoming the most adopted approach. Efforts by D-Wave, Google, IBM and Rigetti, for example, all use superconducting circuits based on Josephson junctions. Notably, IBM allows public access to a subset of their devices through their cloud based Quantum Experience, and additional access to members of their IBM Q network [7].

Quantum computational technology is still in its infancy, with the state-of-the-art in superconducting qubits consisting of approximately a hundred qubits, 99% two-qubit gate fidelities, and coherence times of the order of $100\mu s$ [6]. Fault-tolerant error correction is also currently out of reach, and solutions for quantum memory and networking are not fully developed. They are consequently described as Noisy Intermediate-Scale Quantum (NISQ) devices [8]. There are still unanswered questions about the potential utility of NISQ technology and whether there are fundamental obstructions to going beyond this regime. Nevertheless, there has recently been a flurry of proof-of-principle experiments, along with the recent claim of a demonstrable computational advantage using a quantum computer [9, 10]. For example, in the realm of quantum simulation, real quantum devices have been used to find the ground state of small molecules relevant for quantum chemistry [11, 12], to measure multi-qubit quantum entanglement [13, 14], and to simulate non-equilibrium quantum dynamics [15, 16]. This list is far from exhaustive and we do not intend to review the rapid progress of the last decade.

As realised at the very inception of quantum computing [17], the study of complex many-body quantum systems could benefit tremendously from this new technology. Generically, these systems require the storage and manipulation of an exponentially large number of parameters on a classical computer. By storing and manipulating the quantum state directly on a quantum computer, it may be possible to reach areas of condensed matter physics that are currently intractable. As a relevant example, there does not yet exist a complete classification of topological phases of matter [18]. The most interesting and least understood phases occur in two or three dimensions and host exotic non-abelian anyonic quasiparticles [19], and as a result our most powerful numerical techniques begin to break down. Most notably, quantum Monte Carlo suffers from the sign problem, and dimensionality is a problem for tensor network based methods due to increased entanglement and less efficient contraction schemes when compared with one dimension. On a quantum computer we can avoid classically storing the quantum state, perform sign-problem free computations and work directly with two-dimensional quantum circuits, potentially sidestepping some of the issues plaguing current numerical techniques.

RESULTS

Here, we use the IBM quantum computers to study a symmetry protected topological (SPT) phase of matter [20, 21]. An SPT phase is one that, as long as certain symmetries are present, is not adiabatically connected to a trivial product state. SPTs cannot be understood in

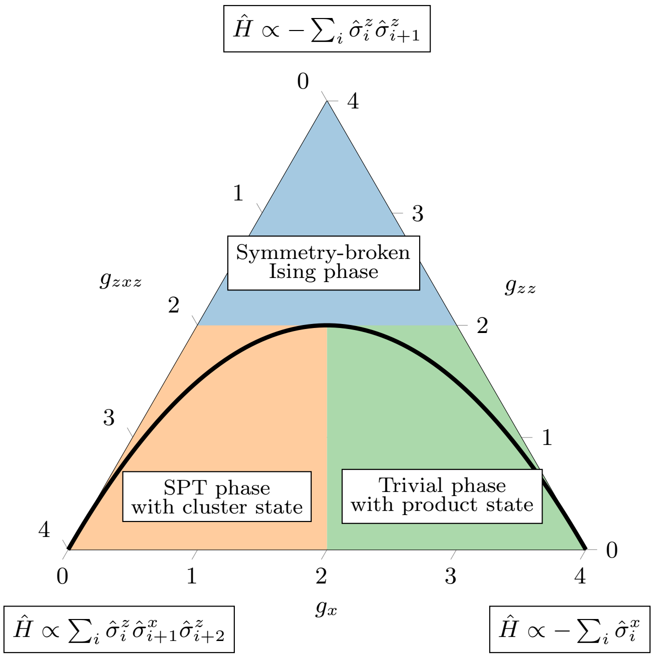

FIG. 1. **Phase diagram for the $\mathbb{Z}_2 \times \mathbb{Z}_2^T$ symmetric Hamiltonian in equation (1).** The green phase is the topologically trivial phase containing the paramagnetic product state, the blue phase is the symmetry-broken phase containing the ferromagnetic ground state of the Ising model and the orange phase is the SPT phase containing the cluster state. The black curve corresponds to the one-dimensional path with tuning parameter g described in the main text.

the framework of local order parameters and spontaneous symmetry breaking. Instead they are distinguished by non-local string order parameters [22–24]. We consider infinite one dimensional spin-$\frac{1}{2}$ chains described by the three parameter Hamiltonian

$$\hat{H} = \sum_i \left[-g_{zz}\, \hat{\sigma}_i^z \hat{\sigma}_{i+1}^z - g_x\, \hat{\sigma}_i^x + g_{zxz}\, \hat{\sigma}_i^z \hat{\sigma}_{i+1}^x \hat{\sigma}_{i+2}^z \right]. \quad (1)$$

This Hamiltonian is symmetric under global spin flips generated by $\prod_i \hat{\sigma}_i^x$ as well as time-reversal. Due to these symmetries the model has a $\mathbb{Z}_2 \times \mathbb{Z}_2^T$ SPT phase, as well as a trivial and a symmetry-broken phase. The phase diagram is shown in Fig. 1 [25, 26].

We focus on a one dimensional path through this phase diagram, corresponding to the black curve in Fig. 1, parametrized as $g_{zz} = 2(1-g^2)$, $g_x = (1+g)^2$ and $g_{zxz} = (g-1)^2$, with tuning parameter g [27]. This path continuously interpolates between the cluster Hamiltonian $\hat{H}_{\mathrm{ZXZ}} = 4\sum_i \hat{\sigma}_i^z \hat{\sigma}_{i+1}^x \hat{\sigma}_{i+2}^z$ for $g=-1$ and the trivial paramagnet with Hamiltonian $\hat{H}_{\mathrm{X}} = -4\sum_i \hat{\sigma}_i^x$ for $g=1$. The transition between the trivial and the SPT phase occurs at the tricritical point between the three phases at $g=0$.

The non-trivial SPT phase can be distinguished using string order parameters [28], which are non-local observables of macroscopic length l. In the limit $l \to \infty$, the string order parameters are non-zero in one of the two phases and zero in the other. The string order parameters that we consider are of the form

$$\mathcal{S}^O(g) = \langle \psi | \hat{O}_i \left(\prod_{j=i+2}^{k-2} \hat{\sigma}_j^x \right) \hat{O}'_k | \psi \rangle \quad (2)$$

with $\hat{O}_i = \hat{\sigma}_i^z \hat{\sigma}_{i+1}^y$ and $\hat{O}'_k = \hat{\sigma}_{k-1}^y \hat{\sigma}_k^z$ defining $\mathcal{S}^{ZY}(g)$, and $\hat{O}_i = \hat{O}'_k = \mathbb{1}$ defining $\mathcal{S}^{\mathbb{1}}$. The length of the string, l, is the distance between the first and last Pauli-operator. Along our path parametrized by g, the string order parameter $\mathcal{S}^{ZY}(g)$ (resp. $\mathcal{S}^{\mathbb{1}}(g)$) is zero for $g>0$ ($g<0$) and equal to $4|g|/(1+|g|)^2$ for $g<0$ ($g>0$). The chosen path has the nice property that the string order parameters are independent of the length of the string and correspond exactly to the values obtained in the thermodynamic limit $l \to \infty$. This property only holds along the black line in Fig. 1 and away from this line we would generically need a macroscopic length l to sharply differentiate the phases.

Infinite state as finite quantum circuit

The ground state of the infinite system can be constructed iteratively by a quantum circuit shown schematically in Fig. 2(a). Any observable with finite connected support can equivalently be measured using the finite quantum circuit in Fig. 2(b) [29]. That is, any measurement of the qubits—excluding the unphysical first and last qubits—is identical to the corresponding measurement of the infinite chain. In particular, we measure the same energy density $\mathcal{E} = -2(g^2+1)$ and values for the string order parameters.

We arrive at the finite circuit in Fig. 2(b) by first viewing a measurement as sandwiching an operator between the quantum circuit (the ket) and the Hermitian conjugate circuit (the bra). Away from the observable that we are measuring we find circuit elements of the form shown in Fig. 3(a). Below the measured operator these will all cancel due to unitarity. While we can't do this for the gates above the measurement, we can construct the gate U_1 as a fixed-point of the iterative circuit. More explicitly, we can reinterpret the circuit in Fig. 3(a) as a transfer matrix $T_{(\beta\beta'),(\alpha\alpha')}$. Similarly, we can consider the circuit in Fig. 3(b) as a vector $V_{(\alpha\alpha')}$. The unitary U_1 is chosen such that $V_{(\alpha\alpha')}$ is the dominant right eigenvector of $T_{(\beta\beta'),(\alpha\alpha')}$ with eigenvalue 1, i.e. the fixed-point vector under repeated application of the transfer matrix. An alternative way to state the cancellation of the unitaries below the measurement is that the dominant left eigenvector of the transfer matrix corresponds to the identity.

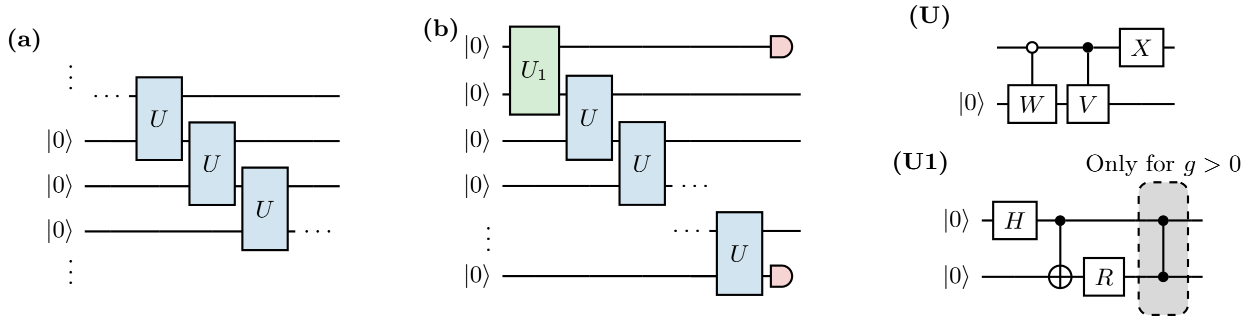

FIG. 2. **Quantum circuit construction of the states**. **(a)** Iterative construction of the ground state on an infinite chain. **(b)** Equivalent finite quantum circuit for measuring observables with finite connected support. Red caps indicate that the end qubits are unphysical and should not be measured. **(U)** and **(U1)** are the circuits for the two-qubit gates U and U_1, respectively. X is the Pauli-X gate, and the single qubit gates R, W and V are specified in the Methods.

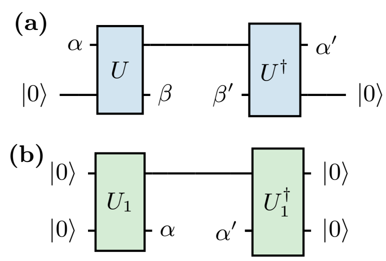

FIG. 3. **Elements of the quantum circuit construction.** **(a)** Circuit element away from measured observable when computing expectation values. This circuit element can be interpreted as a transfer matrix, see main text. **(b)** Corresponding fixed-point vector as a quantum circuit.

Results from the IBM quantum computer

For our simulations we used the 20 qubit IBM Q device codenamed `boeblingen`, which allows the implementation of a universal gate set consisting of arbitrary single qubit rotations and controlled-not (CNOT) entangling gates between connected qubits. The decomposition of the circuit shown in Fig. 2 into this gate set is given in the methods section. The spins in our system are mapped to the physical qubits of the quantum computer, with the basis states $\{|\uparrow\rangle = |0\rangle, |\downarrow\rangle = |1\rangle\}$, and we control the devices using the python qiskit API [30]. To select our subset of N qubits we use a custom procedure described in Ref. [15], which maximizes the average CNOT fidelity, while limiting the readout error and coherence time for the qubits. We also perform error mitigation on the raw data from the machine using methods provided in qiskit [30], which reduces the impact of readout errors. We perform 8192 runs for each circuit and omit errorbars in our figures since the statistical error is not significant.

Figure 4 shows the energy density of the state as measured on the IBM device compared with the analytic value, $\mathcal{E} = -2(g^2 + 1)$. We measure the local energies and average over the central qubits excluding the boundary qubits (i.e. $i = 2, \ldots, N-3$), and show the results for systems of size $N = 5, 6, 7$. Despite the discrepancy in the absolute value, the energy obtained from the quantum computer follows nicely the exact functional form indicating proximity to the target state. However, the accuracy of the results decreases as we increase the system size indicating that we are less faithfully reproducing the larger quantum circuits. This is due to the increased depth resulting in compounded unitary errors and additional decoherence from the longer real-world time for the implementation.

Next we show the measurements of the two string order parameters in Fig. 5 for three lengths, $l = 5, 6, 7$ for $\mathcal{S}^{ZY}(g)$, and $l = 3, 4, 5$ for $\mathcal{S}^{\mathbb{1}}(g)$, and compare with the analytic results. Especially for the smallest system sizes, we see remarkable agreement between the results from the quantum computer and the exact results. As demonstrated in Fig. (5)(a), it appears that we can well approximate the errors in the device by a constant scaling factor. Importantly, the order parameters are only non-zero in one of the two phases, and tend to zero at the phase transition $g = 0$.

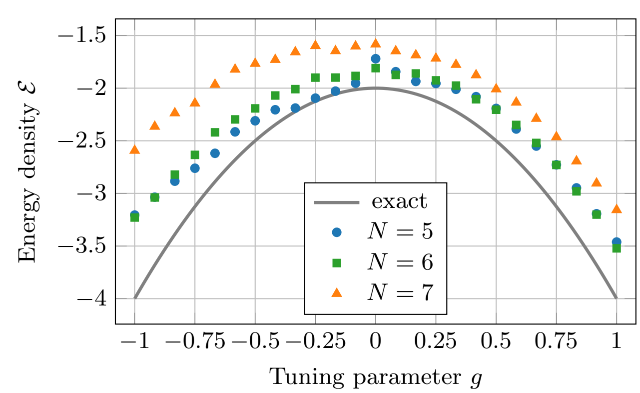

FIG. 4. **Average energy density.** We measure the local energy of the state for systems of length $N = 5, 6, 7$. The energy is averaged over the central sites excluding the end qubits. The data from the IBM devices is compared with the analytic result.

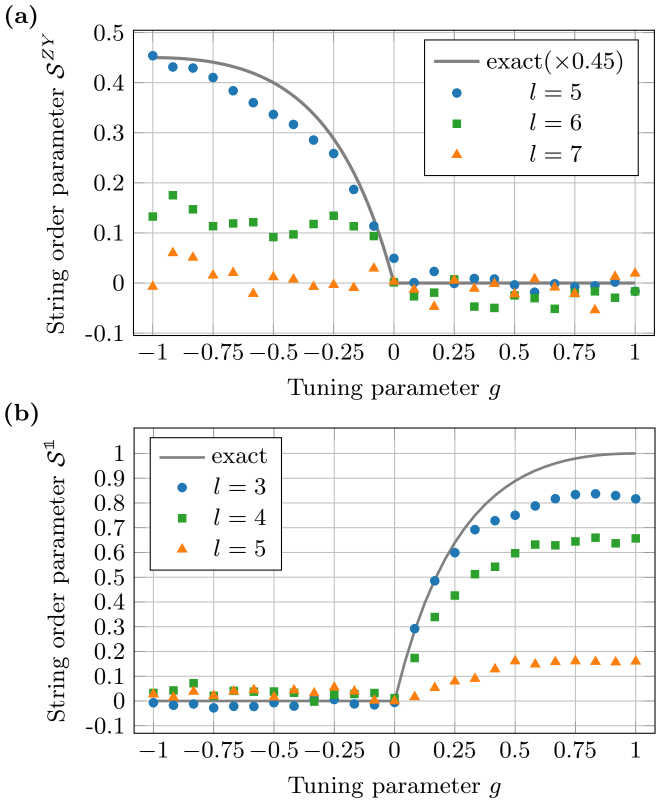

FIG. 5. **Identification of the phase transition.** **(a)** Results of the string order parameter $\mathcal{S}^{ZY}(g)$ of length $l = 5, 6, 7$, measured on systems of size $N = 7, 8, 9$, respectively. **(b)** $\mathcal{S}^{\mathbb{1}}(g)$ of length $l = 3, 4, 5$, on systems of size $N = 5, 6, 7$. We compare with the analytic results, with a constant scaling factor used in **(a)**.

As we increase the system size in Fig. 5, the accuracy of the results quickly diminishes, even more so than was observed in Fig. 4. This is due to the fact that we are measuring non-local operators and both the system size and the length of the operator are increasing. For chains of length $N = 9$ ($l = 7$) we are no longer able to detect the transition, demonstrating the difficulty of constructing and measuring long-range string order in the quantum state due to the current limitations of the quantum computer. Nevertheless, the combination of the measurements of the energy density and the string order parameters confirm that we are able to approximately construct the target states with non-trivial string-order on a real quantum computer.

DISCUSSION

Above we have focused on a particular line through the phase diagram in Fig. 1, which has an especially efficient construction of the ground states. This enabled an exact representation within the limitations of existing devices. In fact, all matrix product states can be constructed in a similar way [29, 31] and can be variationally optimised on a quantum computer [29]. Such variational solvers have already been demonstrated in the setting of small molecules [11, 12] using variational quantum eigensolvers (VQE) [32].

It is still an open and interesting problem to find optimal ansatz circuits for variational optimization. By directly using the connectivity of the quantum computers it may be possible to go beyond what is accessible with classical numerics in two-dimensions with shallow depth (polynomial in system size) quantum circuits. In particular, it is often numerically expensive to compute correlators in higher-dimensional tensor networks. Representing these as quantum circuits [33] will permit considerable speedup in their manipulation and measurement—with a potential exponential advantage in certain circumstances. As a concrete example, there exists a simple representation of topologically ordered string-net models [34] in terms of tensor networks [35, 36], that nevertheless remains difficult to deal with numerically.

Beyond SPT phases, where we know how to construct the order parameters, we need to find efficient ways of detecting and differentiating different phases. Recent work proposes quantum-hybrid algorithms based on ideas from machine learning and renormalization group [37, 38]. These algorithms are scalable and practical to implement on near-term devices. The combination of machine learning tools and quantum hardware is potentially very powerful with many applications [39].

In this paper we have distinguished two topologically inequivalent phases and identified the transition between them using a real quantum device. Despite the infancy of the current technology, our work clearly demonstrates that near-term NISQ devices can be used as practical tools for the study of condensed matter physics.

ACKNOWLEDGEMENTS

We thank Julian Bibo and Ruben Verresen for helpful discussions. Quantum circuit diagrams were produced using the Quantikz latex package [40]. We acknowledge the Samsung Advanced Institute of Technology Global Research Partnership. A.S. and F.P. were in part funded by the European Research Council (ERC) under the European Union's Horizon 2020 research and innovation programme (grant agreement No. 771537). A.G.G was supported by the EPSRC. B.J. was supported by a scholarship from the Hanns-Seidel-Stiftung.

Methods

Quantum circuit in elementary gates

In this section we give the details of the quantum circuit shown schematically in Fig. 2 of the main text. We decompose these circuits into the native gates that can be implemented on the IBM Q devices. The native gates are the single qubit rotations

$$\boxed{U_3(\theta,\phi,\lambda)} = \begin{pmatrix} \cos\frac{\theta}{2} & -e^{i\lambda}\sin\frac{\theta}{2} \\ e^{i\phi}\sin\frac{\theta}{2} & e^{i(\lambda+\phi)}\cos\frac{\theta}{2} \end{pmatrix}. \quad (3)$$

and the controlled-not (CNOT) entangling operation.

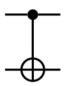

$$= \begin{pmatrix} 1 & 0 & 0 & 0 \\ 0 & 1 & 0 & 0 \\ 0 & 0 & 0 & 1 \\ 0 & 0 & 1 & 0 \end{pmatrix}. \quad (4)$$

We will also use two special single qubit gates

$$\boxed{X} = \begin{pmatrix} 0 & 1 \\ 1 & 0 \end{pmatrix}, \quad \boxed{H} = \frac{1}{\sqrt{2}}\begin{pmatrix} 1 & 1 \\ 1 & -1 \end{pmatrix}, \quad (5)$$

the Pauli-X gate and the Hadamard gate.

The quantum circuits in Fig. 2 contain three two-qubit gates that need to be decomposed further into the elementary gate set. These are all of the form of controlled unitary gates. The first is the controlled-Z or controlled-phase gate

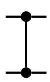 $=$ 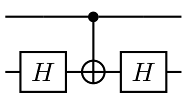 . (6)

The other two are of the form

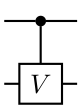 , and 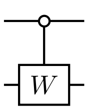 $=$ 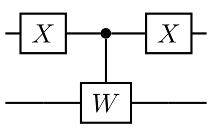 , (7)

where the single qubit gates are of the form

$$V = \begin{pmatrix} \sin\theta_v & \cos\theta_v \\ \cos\theta_v & -\sin\theta_v \end{pmatrix}, \quad (8)$$

and similarly for W. For these single qubit gates the controlled-unitary gate can be implemented using a single CNOT as follows

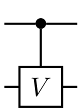 $=$ 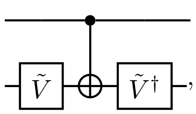 , (9)

where $\tilde{V} = U_3(\theta_v, 0, 0)$ and $\tilde{W} = U_3(\theta_w, 0, 0)$, and $R = U_3(\theta_r, 0, \pi)$ for the gate in Fig. 2(U1), with angles specified by

$$\begin{aligned} \theta_v &= \arcsin\left(\frac{\sqrt{|g|}}{\sqrt{1+|g|}}\right), \quad \theta_v \in [-\pi/2, \pi/2], \\ \theta_w &= \arccos\left(\frac{\mathrm{sign}(g)\sqrt{|g|}}{\sqrt{1+|g|}}\right), \quad \theta_w \in [0, \pi], \\ \theta_r &= 2\arcsin\left(\frac{1}{\sqrt{1+|g|}}\right), \quad \theta_r \in [-\pi, \pi]. \end{aligned} \quad (10)$$

The fully decomposed gates are then shown in Fig. 6.

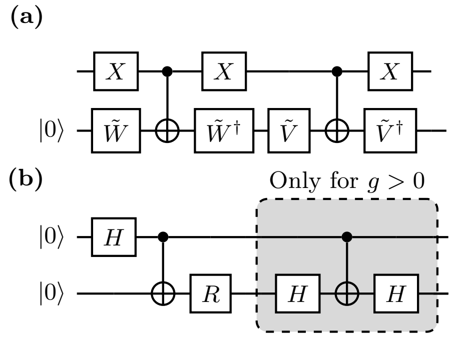

FIG. 6. **Decomposition of the two-qubit gates into the elementary gate set.** **(a)** The quantum circuit of the two-qubit gate U, and **(b)** The quantum circuit of the two-qubit gate $U1$, shown in Fig. 2 in the main text.

* adam.smith@tum.de

[1] Michael A. Nielsen and Isaac L. Chuang, *Cambridge Univ. Press.* (Cambridge University Press, Cambridge, 2010).
[2] Colin D. Bruzewicz, John Chiaverini, Robert McConnell, and Jeremy M. Sage, "Trapped-Ion Quantum Computing: Progress and Challenges," (2019), arXiv:1904.04178.
[3] C. E. Bradley, J. Randall, M. H. Abobeih, R. C. Berrevoets, M. J. Degen, M. A. Bakker, M. Markham, D. J. Twitchen, and T. H. Taminiau, "A Ten-Qubit Solid-State Spin Register with Quantum Memory up to One Minute," Phys. Rev. X **9**, 031045 (2019).
[4] C H Yang, K W Chan, R Harper, W Huang, T Evans, J C C Hwang, B Hensen, A Laucht, T Tanttu, F E Hudson, S T Flammia, K M Itoh, A Morello, S D Bartlett, and A S Dzurak, "Silicon qubit fidelities approaching incoherent noise limits via pulse engineering," Nat. Electron. **2**, 151–158 (2019).
[5] G. Wendin, "Quantum information processing with superconducting circuits: a review," Reports Prog. Phys. **80**, 106001 (2017), arXiv:1610.02208.
[6] Morten Kjaergaard, Mollie E. Schwartz, Jochen Braumüller, Philip Krantz, Joel I-Jan Wang, Simon Gustavsson, and William D. Oliver, "Superconducting Qubits: Current State of Play," (2019), arXiv:1905.13641.

[7] "IBM Q," .

[8] John Preskill, "Quantum Computing in the NISQ era and beyond," Quantum **2**, 79 (2018), arXiv:1801.00862.

[9] Sergio Boixo, Sergei V. Isakov, Vadim N. Smelyanskiy, Ryan Babbush, Nan Ding, Zhang Jiang, Michael J. Bremner, John M. Martinis, and Hartmut Neven, "Characterizing quantum supremacy in near-term devices," Nat. Phys. **14**, 595–600 (2018).

[10] Frank Arute, Kunal Arya, Ryan Babbush, Dave Bacon, Joseph C. Bardin, Rami Barends, Rupak Biswas, Sergio Boixo, Fernando G. S. L. Brandao, David A. Buell, Brian Burkett, Yu Chen, Zijun Chen, Ben Chiaro, Roberto Collins, William Courtney, Andrew Dunsworth, Edward Farhi, Brooks Foxen, Austin Fowler, Craig Gidney, Marissa Giustina, Rob Graff, Keith Guerin, Steve Habegger, Matthew P. Harrigan, Michael J. Hartmann, Alan Ho, Markus Hoffmann, Trent Huang, Travis S. Humble, Sergei V. Isakov, Evan Jeffrey, Zhang Jiang, Dvir Kafri, Kostyantyn Kechedzhi, Julian Kelly, Paul V. Klimov, Sergey Knysh, Alexander Korotkov, Fedor Kostritsa, David Landhuis, Mike Lindmark, Erik Lucero, Dmitry Lyakh, Salvatore Mandrà, Jarrod R. McClean, Matthew McEwen, Anthony Megrant, Xiao Mi, Kristel Michielsen, Masoud Mohseni, Josh Mutus, Ofer Naaman, Matthew Neeley, Charles Neill, Murphy Yuezhen Niu, Eric Ostby, Andre Petukhov, John C. Platt, Chris Quintana, Eleanor G. Rieffel, Pedram Roushan, Nicholas C. Rubin, Daniel Sank, Kevin J. Satzinger, Vadim Smelyanskiy, Kevin J. Sung, Matthew D. Trevithick, Amit Vainsencher, Benjamin Villalonga, Theodore White, Z. Jamie Yao, Ping Yeh, Adam Zalcman, Hartmut Neven, and John M. Martinis, "Quantum supremacy using a programmable superconducting processor," Nature **574**, 505–510 (2019).

[11] Abhinav Kandala, Antonio Mezzacapo, Kristan Temme, Maika Takita, Markus Brink, Jerry M. Chow, and Jay M. Gambetta, "Hardware-efficient variational quantum eigensolver for small molecules and quantum magnets," Nature **549**, 242–246 (2017), arXiv:1704.05018.

[12] P. J.J. O'Malley, R. Babbush, I. D. Kivlichan, J. Romero, J. R. McClean, R. Barends, J. Kelly, P. Roushan, A. Tranter, N. Ding, B. Campbell, Y. Chen, Z. Chen, B. Chiaro, A. Dunsworth, A. G. Fowler, E. Jeffrey, E. Lucero, A. Megrant, J. Y. Mutus, M. Neeley, C. Neill, C. Quintana, D. Sank, A. Vainsencher, J. Wenner, T. C. White, P. V. Coveney, P. J. Love, H. Neven, A. Aspuru-Guzik, and J. M. Martinis, "Scalable quantum simulation of molecular energies," Phys. Rev. X **6** (2016).

[13] Kenny Choo, Curt W. von Keyserlingk, Nicolas Regnault, and Titus Neupert, "Measurement of the Entanglement Spectrum of a Symmetry-Protected Topological State Using the IBM Quantum Computer," Phys. Rev. Lett. **121**, 086808 (2018), arXiv:1804.09725.

[14] Yuanhao Wang, Ying Li, Zhang-qi Yin, and Bei Zeng, "16-qubit IBM universal quantum computer can be fully entangled," npj Quantum Inf. **4**, 46 (2018), arXiv:1801.03782.

[15] Adam Smith, M. S. Kim, Frank Pollmann, and Johannes Knolle, "Simulating quantum many-body dynamics on a current digital quantum computer," (2019), arXiv:1906.06343.

[16] Francesco Tacchino, Alessandro Chiesa, Stefano Carretta, and Dario Gerace, "Quantum computers as universal quantum simulators: state-of-art and perspectives," (2019), arXiv:1907.03505.

[17] Richard P. Feynman, "Simulating physics with computers," Int. J. Theor. Phys. **21**, 467–488 (1982).

[18] Xiao-Gang Wen, "Choreographed entangle dances: topological states of quantum matter," (2019), 10.1126/science.aal3099, arXiv:1906.05983.

[19] Chetan Nayak, Steven H Simon, Ady Stern, Michael Freedman, and Sankar Das Sarma, "Non-Abelian anyons and topological quantum computation," Rev. Mod. Phys. **80**, 1083–1159 (2008), arXiv:arXiv:0707.1889v2.

[20] Frank Pollmann, Ari M. Turner, Erez Berg, and Masaki Oshikawa, "Entanglement spectrum of a topological phase in one dimension," Phys. Rev. B - Condens. Matter Mater. Phys. **81** (2010).

[21] Xie Chen, Zheng Cheng Gu, Zheng Xin Liu, and Xiao Gang Wen, "Symmetry protected topological orders and the group cohomology of their symmetry group," Phys. Rev. B - Condens. Matter Mater. Phys. **87** (2013).

[22] Jutho Haegeman, David Pérez-García, Ignacio Cirac, and Norbert Schuch, "Order Parameter for Symmetry-Protected Phases in One Dimension," Phys. Rev. Lett. **109**, 050402 (2012), arXiv:arXiv:1201.4174v2.

[23] Frank Pollmann and Ari M. Turner, "Detection of symmetry-protected topological phases in one dimension," Phys. Rev. B **86**, 125441 (2012), arXiv:1204.0704.

[24] Andreas Elben, Jinlong Yu, Guanyu Zhu, Mohammad Hafezi, Frank Pollmann, Peter Zoller, and Benoît Vermersch, "Many-body topological invariants from randomized measurements," (2019), arXiv:1906.05011.

[25] Ruben Verresen, Roderich Moessner, and Frank Pollmann, "One-dimensional symmetry protected topological phases and their transitions," Phys. Rev. B **96** (2017).

[26] Ruben Verresen, Nick G. Jones, and Frank Pollmann, "Topology and Edge Modes in Quantum Critical Chains," Phys. Rev. Lett. **120** (2018).

[27] Michael M. Wolf, Gerardo Ortiz, Frank Verstraete, and J. Ignacio Cirac, "Quantum phase transitions in matrix product systems," (2005), 10.1103/PhysRevLett.97.110403, arXiv:0512180 [cond-mat].

[28] D. Pérez-García, M. M. Wolf, M. Sanz, F. Verstraete, and J. I. Cirac, "String order and symmetries in quantum spin lattices," Phys. Rev. Lett. **100** (2008).

[29] Fergus Barratt, Matthias Bal, Vid Stojevic, Frank Pollman, and A. G. Green. *Unpublished*.

[30] Gadi Aleksandrowicz and Et al, "Qiskit: An Open-source Framework for Quantum Computing," (2019).

[31] C. Schön, E. Solano, F. Verstraete, J. I. Cirac, and M. M. Wolf, "Sequential generation of entangled multiqubit states," Phys. Rev. Lett. **95**, 1–5 (2005), arXiv:0501096v1 [arXiv:quant-ph].

[32] Alberto Peruzzo, Jarrod McClean, Peter Shadbolt, Man-Hong Yung, Xiao-Qi Zhou, Peter J. Love, Alán Aspuru-Guzik, and Jeremy L. O'Brien, "A variational eigenvalue solver on a photonic quantum processor," Nat. Commun. **5**, 4213 (2014).

[33] M. C. Bañuls, D. Pérez-García, M. M. Wolf, F. Verstraete, and J. I. Cirac, "Sequentially generated states for the study of two-dimensional systems," Phys. Rev. A - At. Mol. Opt. Phys. **77** (2008).

[34] Michael A Levin and Xiao-Gang Wen, "String-net condensation: A physical mechanism for topological phases,"

Phys. Rev. B **71**, 045110 (2005).

[35] Oliver Buerschaper, Miguel Aguado, and Guifré Vidal, "Explicit tensor network representation for the ground states of string-net models," Phys. Rev. B **79**, 085119 (2009).

[36] Zheng-Cheng Gu, Michael Levin, Brian Swingle, and Xiao-Gang Wen, "Tensor-product representations for string-net condensed states," Phys. Rev. B **79**, 085118 (2009), arXiv:arXiv:0809.2821v1.

[37] Edward Grant, Marcello Benedetti, Shuxiang Cao, Andrew Hallam, Joshua Lockhart, Vid Stojevic, Andrew G. Green, and Simone Severini, "Hierarchical quantum classifiers," npj Quantum Inf. **4** (2018).

[38] Iris Cong, Soonwon Choi, and Mikhail D. Lukin, "Quantum convolutional neural networks," Nat. Phys. (2019).

[39] Jacob Biamonte, Peter Wittek, Nicola Pancotti, Patrick Rebentrost, Nathan Wiebe, and Seth Lloyd, "Quantum machine learning," Nature **549**, 195–202 (2017), arXiv:1611.09347.

[40] Alastair Kay, "Tutorial on the Quantikz Package," (2018), 10.17637/rh.7000520, arXiv:1809.03842.